JOURNAL OF THE ROYAL SOCIETY Interface

Viscoelastic nanoscale properties of cuticle contribute to the high-pass properties of spider vibration receptor (*Cupiennius salei* Keys)

Michael E McConney, Clemens F Schaber, Michael D Julian, Friedrich G Barth and Vladimir V Tsukruk

J. R. Soc. Interface 2007 **4**, 1135-1143
doi: 10.1098/rsif.2007.1000

JOURNAL OF THE ROYAL SOCIETY Interface

J. R. Soc. Interface (2007) **4**, 1135–1143
doi:10.1098/rsif.2007.1000
Published online 3 April 2007

Viscoelastic nanoscale properties of cuticle contribute to the high-pass properties of spider vibration receptor (*Cupiennius salei* Keys)

Michael E. McConney[1,†], Clemens F. Schaber[2,†], Michael D. Julian[3], Friedrich G. Barth[2,*] and Vladimir V. Tsukruk[1,*]

[1]*School of Materials Science and Engineering, Georgia Institute of Technology, Atlanta, GA 30332, USA*
[2]*Department of Neurobiology and Cognition Research, University of Vienna, Althanstraße 14, 1090 Wien, Austria*
[3]*Department of Materials Science and Engineering, Iowa State University, Ames, IA 50011, USA*

Atomic force microscopy (AFM) and surface force spectroscopy were applied in live spiders to their joint pad material located distal of the metatarsal lyriform organs, which are highly sensitive vibration sensors. The surface topography of the material is sufficiently smooth to probe the local nanomechanical properties with nanometre elastic deflections. Nanoscale loads were applied in the proximad direction on the distal joint region simulating the natural stimulus situation. The force curves obtained indicate the presence of a soft, liquid-like epicuticular layer (20–40 nm thick) above the pad material, which has much higher stiffness. The Young modulus of the pad material is close to 15 MPa at low frequencies, but increases rapidly with increasing frequencies approximately above 30 Hz to approximately 70 MPa at 112 Hz. The adhesive forces drop sharply by about 40% in the same frequency range. The strong frequency dependence of the elastic modulus indicates the viscoelastic nature of the pad material, its glass transition temperature being close to room temperature ($25 \pm 2\,^{\circ}\mathrm{C}$) and, therefore, to its maximized energy absorption from low-frequency mechanical stimuli. These viscoelastic properties of the cuticular pad are suggested to be at least partly responsible for the high-pass characteristics of the vibration sensor's physiological properties demonstrated earlier.

Keywords: spider; vibration sensor; metatarsal lyriform organ; force spectroscopy; viscoelastic materials; high-pass characteristics

1. INTRODUCTION

Vibrations play an important role in the lives of spiders, which use them for prey detection, communication during courtship and other behaviours (Rovner & Barth 1981; Barth 1985). The key vibration receptor organ of spiders is the metatarsal organ. It represents a compound or lyriform slit sense organ and belongs to a class of sensory receptors, which are embedded in the spider's exoskeleton and measure the minute strains occurring in it due to muscle activity, haemolymph pressure, vibrations and other types of mechanical stimuli (Barth 2002). The threshold vibrations necessary to elicit a nervous response of the sensory cells supplying individual slits in this organ are known to exhibit pronounced high-pass characteristics, with low sensitivity for frequencies approximately below 30 Hz and steeply increasing threshold sensitivity at higher frequencies (Barth & Geethabali 1982). Other than this change in sensitivity, the organs are not tuned to specific frequencies within the biologically relevant range. The dramatic change in sensitivity was found to be physiologically important for the spider, because it provides filtering of biologically irrelevant background noise, and at the same time preserves much higher sensitivity to biologically relevant vibrations like vibratory courtship signals and vibrations produced by prey motion (Barth 2002).

Located at the distal end of the metatarsus, just distal to the metatarsal lyriform organ, is a pad cushioning the joint between the tarsus and metatarsus (figure 1*a–d*). This pad is crescent shaped and its cuticle is approximately 100 μm thick. It is believed that this pad might be a mechanical source of the physiological high-pass filtering. Substrate vibrations naturally received and transmitted by the tarsus are detected

*Authors for correspondence (friedrich.g.barth@univie.ac.at; vladimir@mse.gatech.edu).
†These authors contributed equally to this work.

Received 8 February 2007
Accepted 14 March 2007

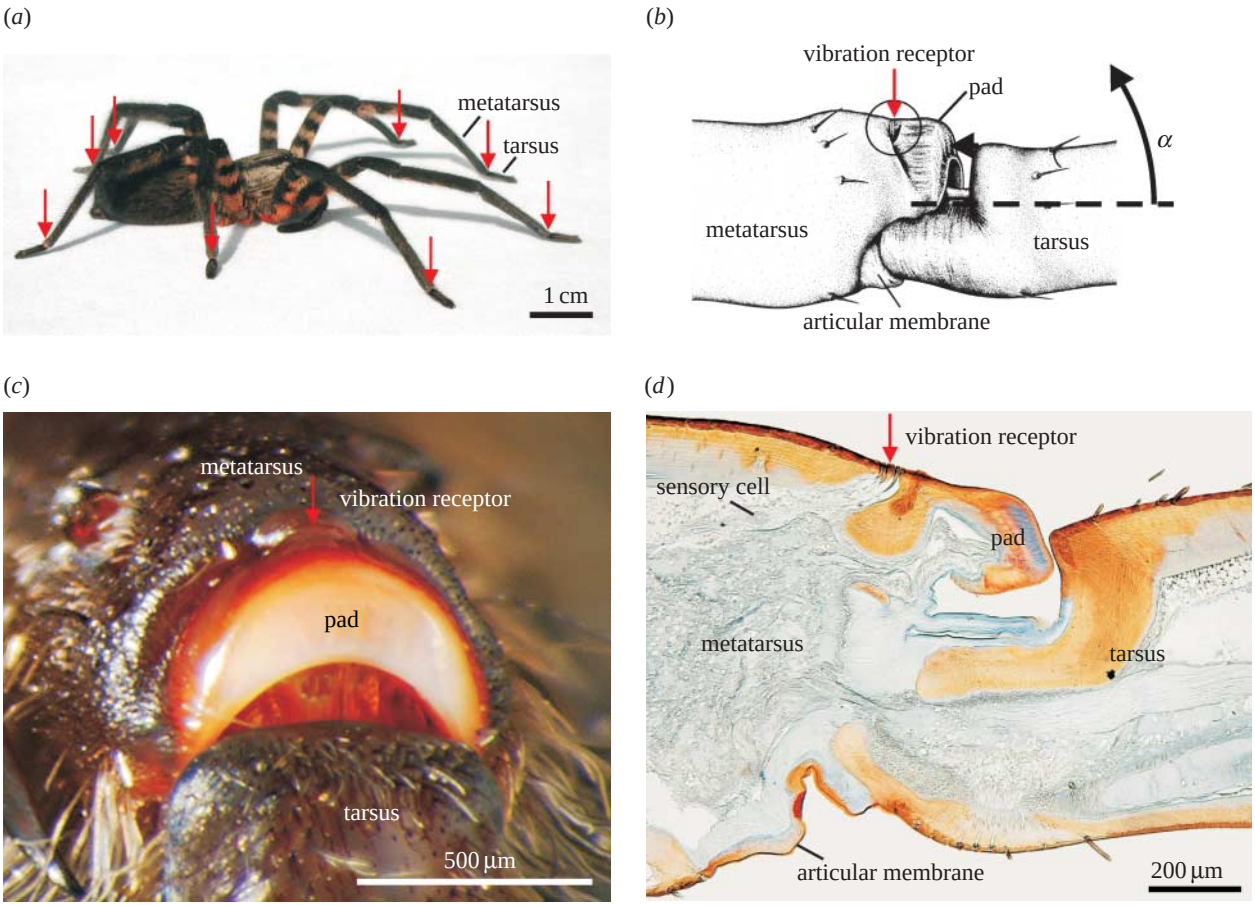

Figure 1. (*a*) Adult female wandering spider, *Cupiennius salei*. The damping pad examined and the vibration receptor organs are located on the metatarsus at the joint with the tarsus (red arrows). (*b*) Deflection of tarsus by an angle α exceeding 25° leads to pressure on the pad in front of the vibration receptor. (*c*) Vibration receptive lyriform organ located between the pad and the stiff cuticle of the metatarsus. (*d*) Sagittal section of the joint, Mallory stained. The pad consists of layers of different types of cuticle; the blue colour indicates soft, moderately sclerotized cuticle. Slits of the vibration receptor are innervated by bipolar sensory cells.

by the slits of the metatarsal lyriform organ when the proximal end of the tarsus pushes against the distal end of the metatarsus, which in turn compresses the slits (figure 1*b*). Therefore, this pad seems ideally placed to mechanically filter the stimuli to the lyriform organ through frequency-dependent damping of the mechanical vibrations. The present study is undertaken to support or reject this hypothesis.

The low forces applied in atomic force microscopy (AFM) and surface force spectroscopy (SFS) allow very soft materials to be probed with nanoscale resolution, while avoiding plastic deformation of the material (Chen & Vlassak 2001; Kovalev *et al.* 2004). There have been several previous studies investigating viscoelastic properties of polymeric and biological materials using AFM (Tsui *et al.* 2000; Bliznyuk *et al.* 2002; Kaliappan & Capella 2005, Chaudhuri *et al.* 2007). There are several nanoindentation studies of the mechanics of insect cuticle on the micrometre scale with forces in the millinewton range (Enders *et al.* 2004; Barbakadze *et al.* 2006). With AFM, the indentation depths are of the order of tens of nanometres under nanonewton forces unlike in conventional microindentation with micrometre indentation depths under micronewton forces. This allows limiting the indentation to the selected surface areas of the material of interest without contributions from surrounding structures or materials. In addition, the small size of the AFM probes (nanometres for regular tips and micrometres for colloidal probes) defines small contact areas (diameters of the order of a fraction of a nanometre or a micrometre) and allows high spatial resolution when probing the material properties across the pad.

2. MATERIALS AND METHODS

Live adult females of *Cupiennius salei* (Ctenidae), which is a large (leg span approx. 10 cm) Central American wandering spider (Barth 2002), were immobilized on a solid substrate and fixed to the stage below the scanning probe. The tarsus of an individual leg was then deflected away from the metatarsus in order to expose the joint pad for the measurements. AFM topographical data and force–distance curves (including SFS) were obtained with a Dimension 3000 microscope (Digital Instruments, Inc.). The AFM images were obtained using established procedures of light-tapping mode scans in air with scan rates below 2 Hz and an overall resolution of 512×512 pixels for

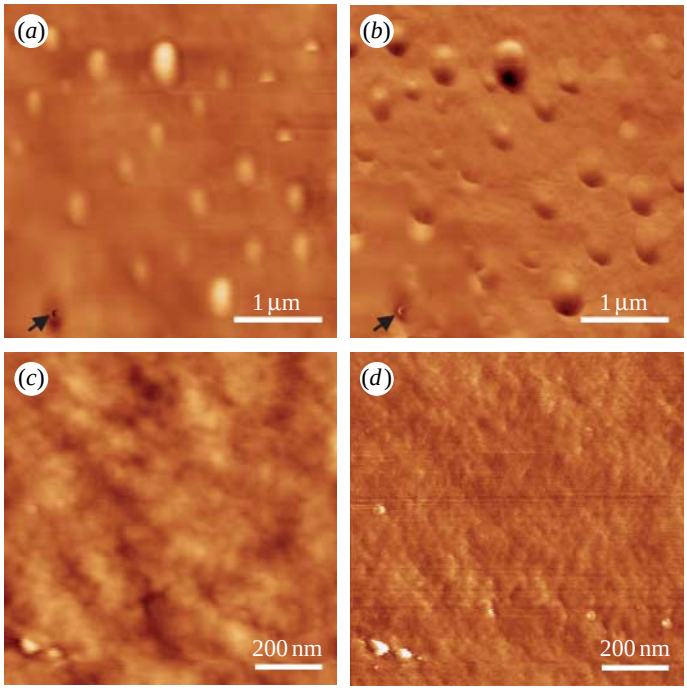

Figure 2. (*a*) AFM height image of the pad surface with 100 nm height range. (*b*) Phase image of the same surface area with 60° phase range. The dome-shaped structures are droplets of epicuticular substances, which are secreted through openings of pore canals. The arrows point to an individual pore canal opening. (*c*) Height image of the pad material at high magnification, 10 nm height range and (*d*) phase image of the same surface area with 30° phase range.

scans ranging from 1×1 to 30×30 µm (Tsukruk & Reneker 1995; Tsukruk 1997). For these scans, standard silicon tips (MikroMasch, NSC11) were used.

The viscoelastic properties of the pad material were probed by acquiring both force–distance curves and force–volume maps using 5 µm spherical borosilicate microsphere probes (Novascan) to reduce local pressure in the contact area. All loads were applied in the proximad direction (similar to natural stimulation) to the distal joint region with the AFM tips approaching and retracting from the pad surface at different velocities. Spring constants were chosen between 1 and 3.6 N m^{-1} (Tsukruk *et al.* 2001). The cantilevers were calibrated applying the accepted spring on spring technique and using a manufacturer calibrated reference tip (MikroMasch) with a spring constant of 4.5 N m^{-1} (Gibson *et al.* 1996; Torii *et al.* 1996).

Force–distance data were collected in air at ambient temperature and humidity in force–volume mode, which included consecutive probing of selected surface areas (16×16 points, number of force–distance curves=256). In this way, multiple force–distance curves were obtained at each surface location and different deflection thresholds studied in order to monitor any changes in the material properties due to plastic deformation by the following AFM scans of the surface area probed. No irreversible changes in the force curve shape were observed during the scans and no indentation marks have been observed after these probings, thus confirming the non-damaging character of our measurements. Force–distance curves were then taken at three to five locations on each joint pad and the data averaged over these locations and thus for several hundred indentations. The frequencies chosen for probing elastic responses (0.1–112 Hz) were limited by the sampling rates of the AFM scanner and its resonant frequencies. However, they cover a significant part of the biologically relevant range, including that of the courtship vibrations (see §3.4; Barth 2002). The pad penetration amplitudes were limited to 30 nm, which should not lead to any plastic deformation when considering the large contact area and the nominal spring constants used in this study. We checked for the presence of indentation marks as indicators of plastic deformation after AFM probing and found none. The temperature during experiments varied between 22 and 24°C only. It was accounted for in the data analysis (uncertainties in the calculated glass transition temperature).

Force–volume analysis was employed according to the established procedures and the measurements analysed with the MMAnalysis software developed by Tsukruk & Gorbunov (2001, 2002). The photodiode sensitivity was measured by pressing the AFM tip against a silicon wafer. The positive deflection of the cantilever seen in the force–distance curves was then converted to indentation depth (penetration) versus loading force (loading curves) using previously described approaches, which consider piezo-element displacement versus tip deflection (Chizhik *et al.* 1998; Tsukruk *et al.* 1998). The data were then analysed for surface stiffness by linear fitting of the slopes. The elastic modulus was calculated from this data by fitting the loading curves according to the Hertzian contact mechanic model, which describes the interactions between the tip and the sample under the assumption of elastic deformation, small contact areas and negligible adhesive forces (Sviridenok *et al.* 1990).

Alternatively, the model of Johnson, Kendall and Roberts (JKR model; Johnson *et al.* 1971), which considers adhesive properties, and Sneddon's model (Sneddon 1965), which considers different tip shapes and the contact areas, were applied to derive the elastic modulus values. However, the results obtained with different models were close to each other and for simplicity we used the results obtained with the Hertzian model. The adhesive forces were determined from force–distance curves at the pull-off point.

Inherently, our force–distance measurements reflect the properties of the topmost layers of the pad structure examined. It is these layers to which we attribute the mechanical filtering described in the present paper. It should be noted that during natural stimulation the forces are introduced basically in the same way.

3. RESULTS AND DISCUSSION

3.1. Surface topography

AFM topographical images confirmed that the surface of the studied pad was consistently smooth with small bumps that are generally uniform and have a diameter of 200–400 nm and a height of 10–30 nm. There are several larger surface bumps as well (figure 2*a*,*b*). The phase image shows the same contrast level for both the surface and the surface bumps, implying that the bumps have similar composition (Leclere *et al.* 2000). The bumps are located above the openings of the pore canals, through which the topmost lipid layers of the epicuticle are secreted. Their distribution matches with that of the pore canals shown in previous transmission electron microscopy studies of the cuticle of *C. salei* (Barth 1969). The mechanical tests were performed so that the tip contact area would include these surface features, because they are included (or the substances smeared in the contact area) as well when the spider's tarsus contacts the pad under natural conditions.

The concurrent high-resolution phase image clearly shows a fine texture of globular aggregates with lateral dimensions below 100 nm (figure 2*c*,*d*). The root mean square (r.m.s.) micro roughness within a 1×1 µm surface area was calculated to be very low at 0.8 nm. This value is on a par with molecularly smooth surfaces with local variations not exceeding two diameters of molecular backbones and very common for soft, amorphous polymeric materials with uniform chemical composition (Tsukruk 1997).

3.2. Force–distance curves

Figure 3 shows typical force–distance curves obtained for the pad material and the same tip probe on a silicon substrate used as a reference surface. The force–distance curve taken for the silicon surface was used to calibrate the sensitivity of the AFM measurements. This curve shows a very linear shape in the region of direct contact between the tip and the surface. A relatively high adhesion (high pull-off forces) is caused by strong capillary interactions between the hydrophilic AFM tip and the hydrophilic substrate under conditions of ambient humidity.

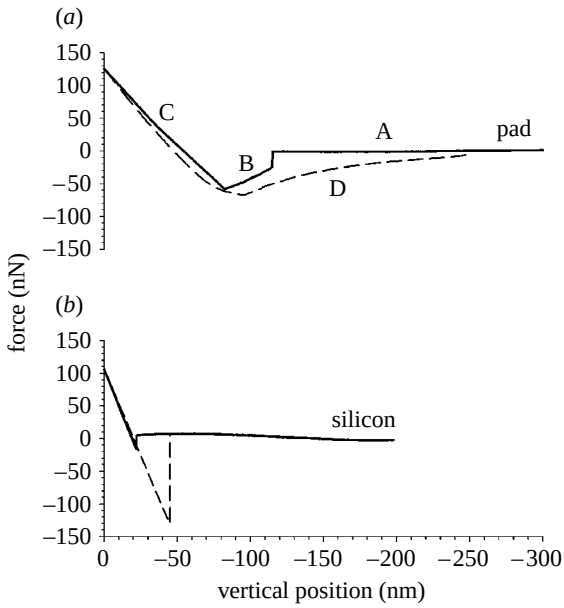

Figure 3. Characteristic force–distance curves obtained for (*a*) the pad material and (*b*) the silicon used for sensitivity calibrations. The solid lines represent data acquired while the tip was approaching the surface and have to be read from right to left according to convention. The dashed lines represent data acquired while the tip was retracting from the surface and have to be read from left to right, again according to convention. Therefore, the start (and end) region is at the right end of the curve, whereas its left end marks the point where the probe tip changes direction. Region A, approaching the sample; region B, contact with the sample; region C, increasing force applied to the sample; region D, adhesive forces between the pad and the tip.

Unlike in the case of the substrate force–distance data for the stiff and hydrophilic silicon, a sharp jump-in event with an extended area of negative tip deflection was consistently observed for the compliant pad surface (region B; figure 3). Direct mechanical contact was followed by a positive deflection (region C) and a broad pull-off region with lower forces (region D). At region A of the curve, the probe is approaching the surface and any attractive forces between the surface and the tip are negligible when compared with the cantilever stiffness thus generating a zero-deflection response. In region B, we see the expected quick jump into contact, followed by a less expected shallow deflection of the cantilever towards the surface, an unusual phenomenon for clean elastic surfaces. This behaviour is indicative of the tip passing through an extremely compliant viscous material that is not slowing its deflection towards the surface, but also generates attractive forces caused by the wetting of the glass probe with the topmost viscous layer (capillary phenomenon). Moreover, its presence is shown on the curve for probe retraction, where instead of a sharp pull-off event, a gradual decrease of adhesive forces is observed, which corresponds to the typical capillary behaviour (region D).

As the AFM probe is withdrawn from the surface, the attractive forces between the probe and the indented surface are overcome by the stiffness of the cantilever and the probe begins to return to its zero-deflection resting point with a gentle deflection finally

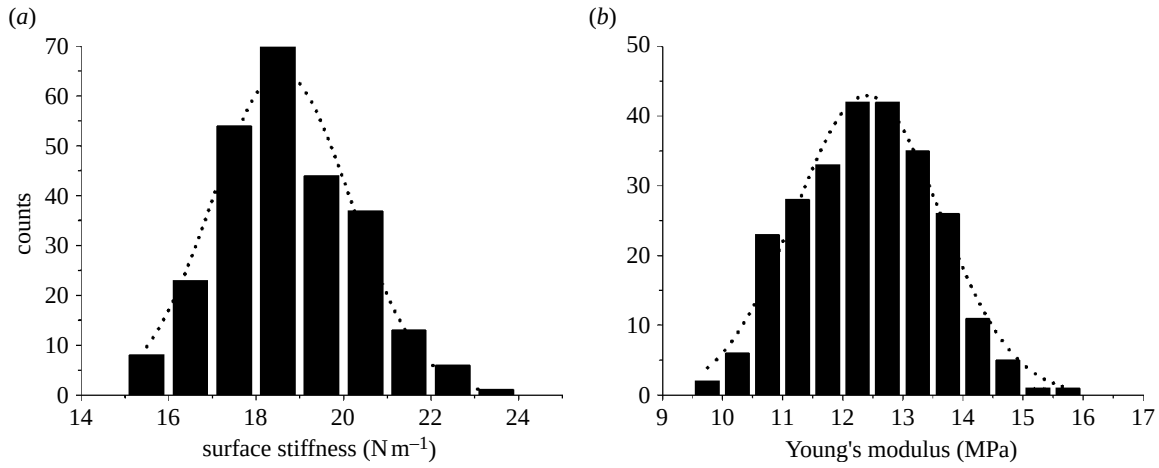

Figure 4. Typical distribution of values for surface stiffness (*a*) and Young's modulus (*b*) for the same pad at 13.9 Hz loading frequency derived from force–volume data taken in a 16×16 array of 1 μm×1 μm (N=1, n=256).

followed by a small sharp 'snap from' region (figure 3). Again, this indicates that the tip is passing through a viscous material and the long-range capillary forces are involved causing gradual thinning of the viscous meniscus before final rupture. The thickness of this surface viscous layer can be estimated from the tip deflection to be within 20–40 nm for different locations and probe frequencies. The appearance of such a viscous surface layer can be directly related to the presence of the oriented lipid layers, which lie above the cuticulin layer and the dense layer of the epicuticle of *C. salei* (Barth 1969). Our data suggest that this topmost viscous layer seen in the force curves is directly related to the bumps seen in figure 1*a*, which could be related to lipid droplets. The bump height is approximately the same as the thickness of the layer indicated by the force curves. Furthermore, there is nothing in region C of the force–distance curves which would indicate that the change in the contact area of the tip with its penetration into the pad is abnormal. In other words, the loading region of the force–distance curves indicates a smooth and flat surface thus pointing to the squeezing of bumps from the contact area during compression. The unexpected behaviour in region B of the force–distance curve, on the other hand, can be fully explained by the presence of the surface bumps.

At the positive slope of the force–distance curves (region C of figure 3, which has to be read from right to left), the tip has made contact with a stiffer elastic material with a measurable resistance to compression. The tip is deflected upwards as the probe pushes into the surface. This is the deformation region of the force curve, which reflects both tip deflection and surface deformation and can be used to analyse the elastic behaviour of the material probed.

3.3. Young's modulus

As mentioned earlier, the force curves indicated that there was significant wetting and adhesion between the tip and pad surface. In such a situation, the Hertzian approximation would tend to underestimate the contact radius, thereby leading to a slightly higher elastic modulus than is the case (usually between 5 and 10% for elastic materials with modest adhesion; Chizhik *et al.* 1998). Generally, a better choice to calculate the elastic modulus of such a material would be the JKR model, which assumes high adhesion (Johnson 1985). As will be discussed later, the adhesion decreased significantly with increased frequencies. This means that when using the JKR model, the change in increase in modulus due to material properties would be slightly exaggerated, whereas using the Hertzian model will slightly underestimate the change in modulus with frequency. Although there was significant adhesion with several of the lower frequency measurements, using the JKR method leads to a more conservative estimation of the material's mechanical filtering abilities. Our estimation showed that for larger elastic deformations, the results obtained from both models (as well as from Sneddon's model) converge, the difference being insignificant for the purpose of this study. Thus, for the sake of clarity and consistency, we applied the Hertzian model to analyse all our data. To this end, we analysed the shapes of the loading curves and fitted them correspondingly for penetrations not usually exceeding 20–30 nm for loading forces below 200 nN. Thirty nanometres of displacement of the pad's dorsal edge corresponds to a change of the angle between metatarsus and tarsus of the spider leg by 0.007° and a displacement of the tarsus tip by about 0.4 μm (Gingl *et al.* 2006). This value represents the sensory threshold of individual slits of the metatarsal organ for substrate vibrations at 70 Hz (slit 6) up to 170 Hz (slit 7; Barth & Geethabali 1982).

Figure 4*a* shows a representative histogram of the surface stiffness data obtained at 13.9 Hz and calculated as the overall slope of the force–distance curve in the direct physical contact regime in linear approximation. The surface stiffness of the pad material at moderate probing frequencies of 13.9 Hz was about 18 N m^{-1} with a distribution in between the range of rubbery and glassy macromolecules (LeMieux *et al.* 2005). The distribution of values of the elastic modulus received for 16×16=256 overlapping locations of a 1 μm^2 area for each spider was very uniform (figure 4*b*). The loading curves (penetration versus loading force) used for fitting analysis were smooth for all surface

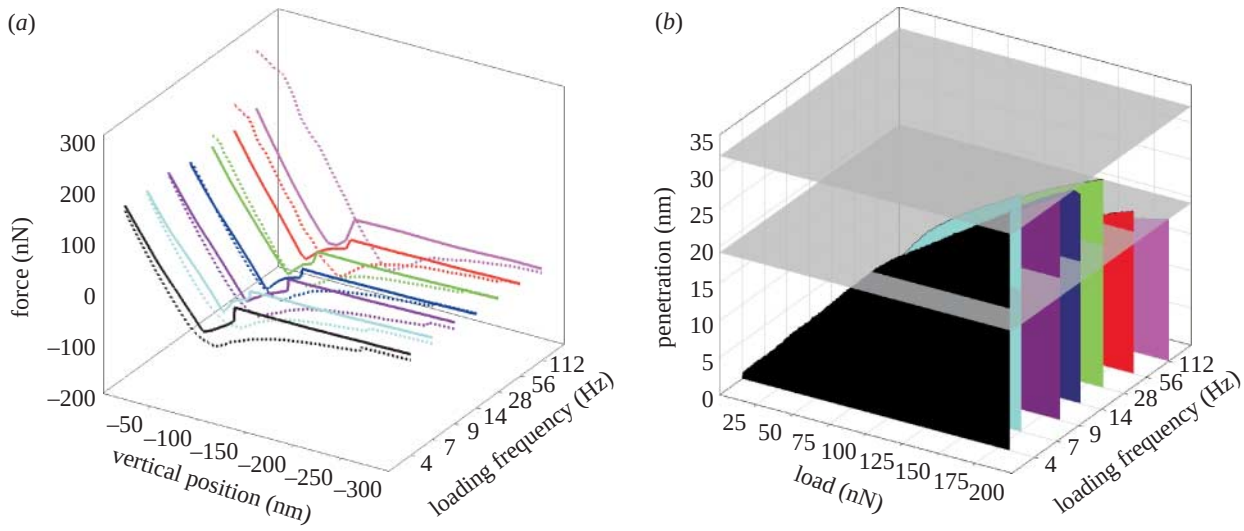

Figure 5. (*a*) Force–distance curves at different probing frequencies; solid lines, approach data; dotted lines, data for the retraction of the probe; the hystereses seen are discussed in the text. (*b*) Loading curves obtained at different frequencies for the pad surface at the same location. The horizontally oriented grey planes are drawn at the maximum penetration at 4 Hz loading frequency and the maximum penetration at 112 Hz loading frequency, respectively.

locations with indentation depths of up to 30–35 nm for loading forces below 200 nN. The value of the elastic modulus for these indentation depths is within a range common for compliant elastic macromolecular materials with low cross-linking density and above the glass transition temperature.[1] The relatively narrow distribution of the surface stiffness (s.d. within $\pm 5\%$ in most cases) indicated a very uniform elastic response of the pad materials under the probed conditions and with the contact area between the probe and the surface below 0.2 μm^2.

3.4. Frequency dependence

Finally, we analysed the mechanical response of the pad surface at different probing frequencies ranging from 0.1 to 112 Hz (the frequency being limited by thermal drifts and piezo-element resonances), corresponding to a tip velocity from very slow (50 nm s^{-1}) to modest (25 $\mu m\ s^{-1}$). Figure 5*a* shows the characteristic force–distance curves obtained at different frequencies and their corresponding loading curves (figure 5*b*). At frequencies below 30 Hz, the force curves obtained have the characteristic shape discussed above with little variance. However, at higher frequencies, this shape changes significantly due to the change of the overall slope. The hysteresis between the approach and retraction curves observed at relatively high probing frequencies is a common AFM artefact. However, it does not significantly affect the measured values derived from the slope of the curve received during intimate contact. Examination of this hysteresis on silicon samples showed that the slope of the force–distance curves changed by less than 5% for this frequency range. This is insignificant when compared with the change of the slope for the pad material itself we observed here. Therefore, the frequency-dependent elastic behaviour is a feature typical of the biological material examined.

Force–distance curves measured at frequencies lower than 10 Hz consistently resulted in values of Young's modulus between 10 and 20 MPa for the pad surfaces of five spiders probed at various locations (figure 6*a*). There was some variance in this value between different specimens; however, the modulus at each spot on the pad varied insignificantly between 0.1 and 10 Hz and all values calculated fell within 15 ± 5 MPa for all varieties of conditions tested. However, above 10 Hz, the value for Young's modulus gradually increased up to 70 MPa for the highest frequencies with a dramatic increase occurring at approximately 30 Hz and higher. Interestingly, the adhesive forces which were very high at low frequency, dropped significantly by approximately 40% in the same frequency range. This confirms the trend towards a more apparently resistant surface, which effectively decreases the contribution of the tip wetting for short contact times (figure 6*c*).

The frequency dependence observed here is attributed to the viscoelastic behaviour of the pad material caused by the time-dependent relaxation of the macromolecular materials in the vicinity of the glass transition (Sperling 1997). In fact, very similar frequency dependencies have been observed for elastomeric materials and were related to the lowered glass transition temperature of the surface caused by the presence of the swollen topmost surface layer (Tsukruk *et al.* 2000). Applying a similar approach allows one to use the time–temperature superposition principle by applying the Williams–Landel–Ferry (WLF) equation (after Sperling 2006) for the evaluation of the glass transition temperature of the pad material. The modulus data at various frequencies were fit using the universal WLF constants C_1 and C_2 as 17.44 and 51.6 as is common for amorphous macromolecular materials

[1]Viscoelastic materials simultaneously exhibit a combination of elastic and viscous behaviour. In polymers the transition that separates the glassy state from the viscous state is known as the glass–rubber transition. In the range of this glass transition the stiffness of a polymer typically drops by a factor of about 1000 with a rise of temperature of 20 to 30°C (Sperling 2006).

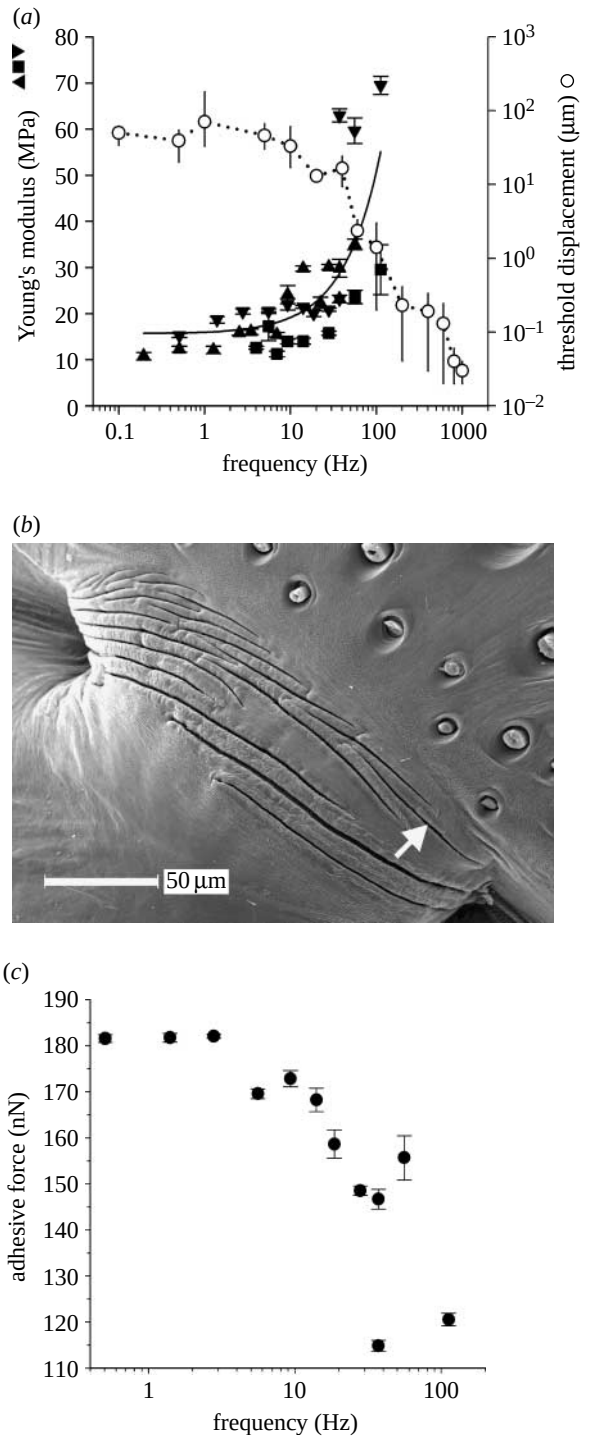

Figure 6. (*a*) Frequency dependence of Young's modulus (filled symbols) and of sensory thresholds of slit 7 of the metatarsal lyriform organ (open circles). The different datasets of Young's modulus are from three locations on joint pads of two spiders. Each data point represents 10–15 force–distance curves. Sensory threshold curve adapted from Barth & Geethabali (1982; $n=16$). (*b*) SEM micrograph of the metatarsal organ of *C. salei* (picture by R. Müllan). The arrow points to slit 7. (*c*) Adhesive forces measured at different loading frequencies at one location of a joint pad.

and applied here to the cuticular matrix. By using this approach, we estimated the glass transition temperature of the joint pad material to be 25 ± 2°C, which is very close to the room temperature prevailing during our experiments (22–24°C).

Thus, the change of the elastic modulus with shorter contact times follows common trends well known for viscoelastic macromolecular materials in the vicinity of the glass transition temperature (Sperling 1997). Upon elastic deformation of any material, some of the energy is stored and some of it is lost in the form of heat, or essentially absorbed. The storage modulus is a measure of the amount of energy stored upon deformation, whereas the loss modulus is a measure of the amount of energy released as heat upon deformation. The ratio of energy absorbed to energy stored reaches a maximum right in the vicinity of the glass transition region, which constitutes a viscoelastic damping phenomenon. When the temperature of a material goes below the glass transition temperature or the deformation rate becomes faster than the polymer's relaxation time, the elastic modulus dramatically increases. Therefore, materials with a glass transition temperature near the intended operating conditions, such as the spider's pad in the vicinity of room temperature, make very good energy absorbing materials with maximum energy dissipation at low frequencies (Sperling 1997).

Importantly, the frequency dependence of the elastic response observed here for the pad material is opposite to the frequency dependence of the sensory threshold reported previously for the metatarsal lyriform organ (Barth & Geethabali 1982; figure 6*a*,*b*). The deflection of the tarsus needed to elicit a nervous response (action potential) measured approximately between 100 and 10 μm at vibration frequencies up to 40 Hz and dropped steeply to values as low as 0.01–0.001 μm at 1 kHz (Barth 1998). The frequencies of wind-induced vibrations of the leaves of the dwelling plants of *C. salei* are significantly lower than 30 Hz. On banana plants and bromeliads, they do not exceed 7 Hz (Barth *et al.* 1988*a*). However, for higher frequencies of mechanical perturbations, such as prey-generated substrate vibrations or the vibratory signals of a sexual partner, the viscoelastic pad material partially loses its viscous nature effectively becoming stiffer, and thus transmitting external mechanical stimuli with higher efficiency (low dissipation). Vibrations of the dwelling plants of *C. salei* induced by prey, like a crawling cockroach, have a broad frequency spectrum containing frequencies higher than 200 Hz. Male abdominal courtship vibrations peak at approximately 75 Hz, whereas male drumming and scratching on the leaf results in vibrations of 250 Hz and higher. The dominant frequency of the female courtship vibration answering male signals is about 30 Hz (Barth 1998, 2002).

The average daily temperatures in the habitats of *C. salei* in Central America are around 20°C, with frequent daily maxima above 30°C all the year round (Barth *et al.* 1988*b*). During the day, when the ambient temperature is high, the spiders rest hidden in their retreats on the dwelling plants. Their hunting activity starts after sunset when the temperature is moderate, but well in the region of the glass transition temperature of the metatarsal pad. Owing to the lowered temperature at night the pad should be stiffer, and the metatarsal vibration receptive organ more sensitive to vibrations than during the rest period of the spider.

The mechanical filter properties described in this study will be useful by keeping the low frequencies (typical of biologically irrelevant stimuli) out of the nervous system, thereby enhancing the signal-to-noise ratio as was already argued in regard to the electrophysiologically determined threshold curves (review in Barth 2002). The mechanical filter does not exclude additional physiological filters whose presence follows from the transfer functions determined for the cells of other slit sense organs (Bohnenberger 1981; French *et al.* 2001).

4. CONCLUSIONS

Spiders strongly rely on substrate vibrations for the guidance of prey capture, predator avoidance and mating behaviour. These signals must be separated from the environmental noise. The most important vibration receptor organ in spiders is the metatarsal lyriform organ, which is relatively insensitive at frequencies below 30 Hz, but increasingly sensitive at higher frequencies. When deflected by vibrations, the tarsus first transmits the stimulus to a soft material pad, which in turn passes it on to the metatarsal vibration sensor immediately behind it. The pad material was found to be highly viscoelastic with its highest compliance and high energy dissipation at frequencies below 30 Hz. At frequencies above 30 Hz, the pad material quickly becomes stiffer, which allows better transmission of vibrations to the metatarsal lyriform organ. The temperature of the pad material was found to be near glass transition, where the energy absorption is maximized. However, if the deformation time is relatively short, the vibration frequency is relatively high, or the temperature is well below the glass transition temperature, the pad material becomes stiffer. Under these conditions, the effective Young's modulus will increase and mechanical losses will go down tremendously. These properties of the pad material make it an ideal high-pass filter, which filters out environmental noise and makes the frequency range of vibrations relevant for the spider most effective.

This work was supported by a grant from the US Defense Advanced Research Projects Agency (DARPA) project BioSenSE FA9550-05-1-0459 to F.G.B. and V.V.T., and by project P16348 of the Austrian Science Foundation (FWF) to F.G.B.

REFERENCES

Barbakadze, N., Enders, S., Gorb, S. & Arzt, E. 2006 Local mechanical properties of the head articulation cuticle in the beetle *Pachnoda marginata* (Coleoptera, Scarabaeidae). *J. Exp. Biol.* **209**, 722–730. (doi:10.1242/jeb.02065)

Barth, F. G. 1969 Die Feinstruktur des Spinnenintegruments I. Die Cuticula des Laufbeins adulter häutungsferner Tiere (*Cupiennius salei* Keys). *Z. Zellforsch.* **97**, 137–159. (doi:10.1007/BF00331877)

Barth, F. G. 1985 Neuroethology of the spider vibration sense. In *Neurobiology of arachnids* (ed. F. G. Barth), pp. 203–229. Berlin, Germany; New York, NY; Tokyo, Japan: Springer.

Barth, F. G. 1998 The vibrational sense of spiders. In *Comparative hearing: insects* (eds R. R. Hoy, A. N. Popper & R. R. Fay), pp. 228–278. New York, NY: Springer.

Barth, F. G. 2002 *A Spider's world: senses and behavior.* Berlin, Germany; New York, NY: Springer.

Barth, F. G. & Geethabali 1982 Spider vibration receptors: threshold curves of individual slits in the metatarsal lyriform organ. *J. Comp. Physiol. A* **148**, 175–185. (doi:10.1007/BF00619124)

Barth, F. G., Bleckmann, H., Bohnenberger, J. & Seyfarth, E.-A. 1988*a* Spiders of the genus *Cupiennius* Simon 1891 (Araneae, Ctenidae) II. On the vibratory environment of a wandering spider. *Oecologia* **77**, 194–201. (doi:10.1007/BF00379186)

Barth, F. G., Seyfarth, E.-A., Bleckmann, H. & Schüch, W. 1988*b* Spiders of the genus *Cupiennius* Simon 1891 (Araneae, Ctenidae) I. Range distribution, dwelling plants, and climatic characteristics of the habitats. *Oecologia* **77**, 187–193. (doi:10.1007/BF00379185)

Bliznyuk, V. N., Assender, H. E. & Briggs, G. A. D. 2002 Surface glass transition temperature of amorphous polymers: a new insight with SFM. *Macromolecules* **35**, 6613–6622. (doi:10.1021/ma011326a)

Bohnenberger, J. 1981 Matched transfer characteristics of single units in a compound slit sense organ. *J. Comp. Physiol. A* **142**, 391–402. (doi:10.1007/BF00605451)

Chaudhuri, O., Parekh, S. H. & Fletcher, D. A. 2007 Reversible stress softening of actin networks. *Nature* **445**, 295–298. (doi:10.1038/nature05459)

Chen, X. & Vlassak, J. J. 2001 Numerical study on the measurement of thin film mechanical properties by means of nanoindentation. *J. Mater. Res.* **16**, 2974–2982.

Chizhik, S. A., Huang, Z., Gorbunov, V. V., Myshkin, N. K. & Tsukruk, V. V. 1998 Micromechanical properties of elastic polymeric materials as probed by scanning force microscopy. *Langmuir* **14**, 2606–2609. (doi:10.1021/la980042p)

Enders, S., Barbakadse, N., Gorb, S. N. & Arzt, E. 2004 Exploring biological surfaces by nanoindentation. *J. Mater. Res.* **19**, 880–887. (doi:10.1557/jmr.2004.0114)

French, A. S., Höger, U., Sekizawa, S. & Torkkeli, P. H. 2001 Frequency response functions and information capacities of paired spider mechanoreceptor neurons. *Biol. Cybern.* **85**, 293–300. (doi:10.1007/s004220100260)

Gibson, C. T., Watson, G. S. & Myhra, S. 1996 Determination of the spring constants of probes for force microscopy/spectroscopy. *Nanotechnology* **7**, 259–262. (doi:10.1088/0957-4484/7/3/014)

Gingl, E., Burger, A.-M. & Barth, F. G. 2006 Intracellular recording from a spider vibration receptor. *J. Comp. Physiol. A* **192**, 551–558. (doi:10.1007/s00359-005-0092-3)

Johnson, K. L. 1985 *Contact mechanics.* Cambridge, UK: Cambridge University Press.

Johnson, K. L., Kendall, K. & Roberts, A. D. 1971 Surface energy and the contact of elastic solids. *Proc. R. Soc. A* **324**, 301–313. (doi:10.1098/rspa.1971.0141)

Kaliappan, S. N. & Capella, B. 2005 Temperature dependent elastic-plastic behavior of polystyrene studied using AFM force-distance curves. *Polymer* **46**, 11 416–11 423. (doi:10.1016/j.polymer.2005.09.066)

Kovalev, A., Shulha, H., LeMieux, M., Myshkin, N. & Tsukruk, V. V. 2004 Nanomechanical probing of layered nanoscale polymer films with atomic force microscopy. *J. Mater. Res.* **19**, 716–728. (doi:10.1557/jmr.2004.0092)

Leclere, P., Bredas, J. L., Moineau, G., Minet, M., Dubois, P., Jerome, R. & Lazzaroni, R. 2000 Microphase separation and morphological transitions at the surface of block co-polymers. In *Microstructure and microtribology of*

polymer surfaces (eds V. V. Tsukruk & K. J. Wahl), pp. 356–368. Washington, DC: American Chemical Society.

LeMieux, M. C., Lin, Y. H., Cuong, P. D., Ahn, H. S., Zubarev, E. R. & Tsukruk, V. V. 2005 Microtribological and nanomechanical properties of switchable y-shaped amphiphilic polymer brushes. *Adv. Funct. Mater.* **15**, 1529–1540. (doi:10.1002/adfm.200500088)

Rovner, J. S. & Barth, F. G. 1981 Vibratory communication through living plants by a tropical wandering spider. *Science* **214**, 464–466. (doi:10.1126/science.214.4519.464)

Sneddon, I. N. 1965 The relation between load and penetration in the axisymmetric boussinesq problem for a punch of arbitrary profile. *Int. J. Eng. Sci.* **3**, 47–57. (doi:10.1016/0020-7225(65)90019-4)

Sperling, L. H. 1997 *Polymeric multicomponent materials: an introduction*. New York, NY: Wiley.

Sperling, L. H. 2006 *Introduction to physical polymer science*, 4th edn. Hoboken, NJ: Wiley.

Sviridenok, A. I., Chizhik, S. A. & Petrokovets, M. I. 1990 *Mechanics of a discrete friction contact*. Minsk, Russia: Nauki I Tekhnika.

Torii, A., Sasaki, M., Hane, K. & Okuma, S. 1996 A method for determining the spring constant of cantilevers for atomic force microscopy. *Meas. Sci. Technol.* **7**, 179–184. (doi:10.1088/0957-0233/7/2/010)

Tsui, O. K. C., Wang, X. P., Ho, J. Y. L., Ng, T. K. & Xiao, X. 2000 Studying surface glass-to-rubber transition using atomic force microsopic adhesion measurements. *Macromolecules* **33**, 4198–4204. (doi:10.1021/ma991473x)

Tsukruk, V. V. 1997 Scanning probe microscopy of polymer surfaces. *Rubber Chem. Technol.* **70**, 430–467.

Tsukruk, V. V. & Gorbunov, V. V. 2001 Nanomechanical probing with scanning force microscopy. *Microsc. Today* **9**, 8–14.

Tsukruk, V. V. & Gorbunov, V. V. 2002 Nanomechanical analysis of polymer surfaces. *Probe Microsc.* **2**, 241–247. (doi:10.1080/13551850214942)

Tsukruk, V. V. & Reneker, D. H. 1995 Scanning probe microscopy of organic and polymeric films: from self-assembled monolayers to composite multilayers. *Polymer* **36**, 1791–1808. (doi:10.1016/0032-3861(95)90925-R)

Tsukruk, V. V., Huang, Z., Chizhik, S. A. & Gorbunov, V. V. 1998 Probing of micromechanical properties of compliant polymeric materials. *J. Mater. Sci.* **33**, 4905–4909. (doi:10.1023/A:1004457532183)

Tsukruk, V. V., Gorbunov, V. V., Huang, Z. & Chizhik, S. 2000 Dynamic microprobing of viscoelastic polymer properties. *Polym. Int.* **49**, 441–444. (doi:10.1002/(SICI)1097-0126(200005)49:5<441::AID-PI240>3.0.CO;2-U)

Tsukruk, V. V., Sidorenko, A., Gorbunov, V. V. & Chizhik, S. A. 2001 Surface nanomechanical properties of polymer nanocomposite layers. *Langmuir* **17**, 6715–6719. (doi:10.1021/la010761v)